

# Tensor numerical method for optimal control problems constrained by an elliptic operator with general rank-structured coefficients

Boris N. Khoromskij\*      Britta Schmitt†      Volker Schulz‡

May 28, 2021

## Abstract

We introduce tensor numerical techniques for solving optimal control problems constrained by elliptic operators in  $\mathbb{R}^d$ ,  $d = 2, 3$ , with variable coefficients, which can be represented in a low rank separable form. We construct a preconditioned iterative method with an adaptive rank truncation for solving the equation for the control function, governed by a sum of the elliptic operator and its inverse  $M = A + A^{-1}$ , both discretized over large  $n^{\otimes d}$ ,  $d = 2, 3$ , spatial grids. Two basic solution schemes are proposed and analyzed. In the first approach, one solves iteratively the initial linear system of equations with the matrix  $M$  such that the matrix vector multiplication with the elliptic operator inverse,  $y = A^{-1}u$ , is performed as an embedded iteration by using a rank-structured solver for the equation of the form  $Ay = u$ . The second numerical scheme avoids the embedded iteration by reducing the initial equation to an equivalent one with the polynomial system matrix of the form  $A^2 + I$ . For both schemes, a low Kronecker rank spectrally equivalent preconditioner is constructed by using the corresponding matrix valued function of the anisotropic Laplacian diagonalized in the Fourier basis. Numerical tests for control problems in 2D setting confirm the linear-quadratic complexity scaling of the proposed method in the univariate grid size  $n$ . Further, we numerically demonstrate that for our low rank solution method, a cascadic multigrid approach reduces the number of PCG iterations considerably, however the total CPU time remains merely the same as for the unigrid iteration.

## 1 Introduction

Optimization problems that are constrained by partial differential equations (PDEs) have a long history in mathematical literature since they arise in a wide range of applications in different fields of natural science, see for example [31, 1, 19] for some comprehensive examples and related references. Being studied for many years, tracking-type problems

---

\*Max-Planck-Institute for Mathematics in the Sciences, Inselstr. 22-26, D-04103 Leipzig, Germany (bokh@mis.mpg.de); Trier University, FB IV - Department of Mathematics, D-54296, Trier, Germany.

†Trier University, FB IV - Department of Mathematics, D-54296, Trier, Germany (schmittb@uni-trier.de).

‡Trier University, FB IV - Department of Mathematics, D-54296, Trier, Germany (volker.schulz@uni-trier.de).

which trace the discrepancy between the solution of the PDE and a given target state represent a very important class of optimal control problems [10]. Among others, a particular class of applications is related to structural topology optimization. In such problems the discretization and numerical treatments of the elliptic PDE in constraints, that determines the relation between the optimal design  $y$  and control function  $u$ ,

$$Ay := \operatorname{div} a(x) \operatorname{grad} y = u, \quad x \in \mathbb{R}^d, \quad (1.1)$$

can be performed by the traditional FEM methods dealing with sparse matrices. In cases when the entire problem can be reduced to the explicit equation for the control function, the system matrix includes the weighted sum of the initial operator  $A$  and its nonlocal inverse  $A^{-1}$ ,  $A + A^{-1}$ . The numerical solution of the resultant equation in multidimensional setting becomes the challenging problem due to the treatment of the fully populated matrix  $A^{-1}$ .

In this way, the multigrid methods for elliptic equations proved to be the efficient option in the context of control problems since they apply to the case of rather general equation coefficients, while the numerical complexity scales linearly in the number of grid points in the computational domain in  $\mathbb{R}^d$ , see [7, 8]. However, the multigrid approach for equations with nonlocal operators of the form  $A + A^{-1}$  does not provide the uniform convergence rate since both the smooth and highly oscillating eigen-functions correspond to large eigenvalues,  $\lambda + \lambda^{-1}$ . In this situation we propose to use a PCG iteration with a spectrally equivalent preconditioner of low Kronecker rank (K-rank) applied to the system matrix  $A + A^{-1}$ .

In the recent decade, tensor numerical methods proved to provide an efficient strategy for large scale computer simulations of PDE driven mathematical models [15, 24, 23]. In particular, the basic numerical multilinear algebra algorithms for the Tucker, canonical, TT and QTT tensors have been described in [9, 16, 15, 24] (see also references therein). Iterative methods for solving linear systems in the rank-structured tensor formats have been considered in particular in [26, 11].

Recently the numerical analysis of optimal control problems constrained by space-fractional elliptic operators was intensively discusses in the literature [2, 21, 12, 18, 29, 3, 5, 10], see also papers on the discretization and analysis of fractional PDEs [13, 17] and [28, 27, 4].

In the present paper we introduce tensor numerical techniques for solving optimal control problems constrained by elliptic operators in  $\mathbb{R}^d$ ,  $d = 2, 3$ , with variable coefficients, which can be represented in low rank separable form. We construct a preconditioned iterative method with an adaptive rank truncation for solving the equation for the control function, governed by a sum of the elliptic operator and its inverse  $M = A + A^{-1}$ , both discretized over large  $n^{\otimes d}$ ,  $d = 2, 3$ , spatial grids. The low-rank approximation of matrix-valued functions and the adaptive rank-truncation in PCG iteration for 3D case can be performed by the multigrid Tucker approximation scheme [25], while for 2D problems we use the standard reduced SVD. Two basic solution schemes are proposed and analyzed.

In the first approach, one can solve iteratively the initial linear system of equations with the system matrix  $M$  such that the matrix vector multiplication with the elliptic operator inverse,  $y = A^{-1}u$ , is performed by solving the equation  $Ay = u$  via the embedded PCG iteration by using algorithms based on multilinear operations on rank-structured data. The second numerical scheme avoids the embedded iteration by transforming the initial equation to the equivalent one with a polynomial system matrix of the form  $AM = A^2 + I$ . For

both approaches, a low Kronecker rank spectrally equivalent preconditioner is constructed by using the reciprocal matrix valued function of the anisotropic Laplacian diagonalized in the Fourier basis. Throughout this work, we refer to the *anisotropic Laplacian* whenever we use a scaled version of the classic Laplace operator  $\Delta$  of the form  $A = \sum_{\ell=1}^d a_{\ell} \frac{\partial^2}{\partial x_{\ell}^2}$ , where the positive constants  $a_1, \dots, a_d$  may vary on different scales. Numerical examples confirm the log-linear complexity scaling of the proposed method in the univariate grid size  $n$ . For a large univariate grid size  $n$  the additional complexity term of the order of  $O(n^2)$  can be observed, which is due to the cost of matrix-vector multiplication.

In order to numerically enhance the pcg iteration scheme, we make use of a cascadic multigrid approach, that means the iterative pcg method on the grid of size  $n \times n$  starts with an interpolation of the solution from the previous grid  $\frac{n}{2} \times \frac{n}{2}$  and no coarse grid correction is done, see [30, 6] for more details.

The rest of the paper is organized as follows. In Section 2 we describe in detail the low Kronecker rank discrete form of elliptic operators with rank- $R$  separable coefficients and then set up the equation for the control function. Section 3 presents the construction and analysis of low rank spectrally equivalent preconditioners. In Section 4 we discuss the computational complexity. In particular, we present numerical study of the presented tensor-based solver applied to control problems constrained by the 2D elliptic equations with variable coefficients. Section 5 concludes the paper.

## 2 Low rank discrete form of elliptic operators with rank- $R$ separable coefficients

In the following, we introduce the target class of tracking-type optimal control problems that motivates our work. Subsequently, the discretization of the target elliptic operator and the effect of separable variables on the structure of the system matrix are presented. Finally, at the end of the chapter, the equation for the problem-specific control is given and analyzed.

Given the design function  $y_{\Omega} \in L^2(\Omega)$  on  $\Omega := (0, 1)^d$ ,  $d = 1, 2, 3$ , first, we consider the optimization problem for the cost functional

$$\min_{y, u} J(y, u) := \frac{1}{2} \int_{\Omega} (y(x) - y_{\Omega}(x))^2 dx + \frac{\gamma}{2} \int_{\Omega} u^2(x) dx, \quad \gamma > 0, \quad (2.1)$$

constrained by the elliptic boundary value problem in  $\Omega$  for the state variable  $y \in H_0^1(\Omega)$ ,

$$\mathcal{A}y := -\nabla^T \cdot \mathbb{A}(x)\nabla y = u, \quad x \in \Omega, \quad u \in L_2(\Omega), \quad (2.2)$$

endorsed with the homogeneous Dirichlet boundary conditions on  $\Gamma = \partial\Omega$ , i.e.,  $y|_{\Gamma} = 0$ . The diagonal  $d \times d$  coefficient matrix takes the form  $\mathbb{A}(x) = \text{diag}\{a(x), \dots, a(x)\} \in \mathbb{R}^{d \times d}$ .

We consider optimal control problems with an elliptic operator in the constraint equation (2.2) that has rank-1 separable variable coefficients in the form

$$\mathcal{A} = - \sum_{\ell=1}^d \frac{d}{dx_{\ell}} \prod_{m=1}^d a_m(x_m) \frac{d}{dx_{\ell}}, \quad x \in (0, 1)^d, \quad (2.3)$$

and the generalization to the rank- $R$  variable coefficients leading to

$$\mathcal{A} = - \sum_{\ell=1}^d \frac{d}{dx_{\ell}} \left( \sum_{k=1}^R \prod_{m=1}^d a_m^{(k)}(x_m) \right) \frac{d}{dx_{\ell}}, \quad x \in (0, 1)^d. \quad (2.4)$$

## 2.1 Galerkin stiffness matrix in tensor product basis

To enhance the application of the Kronecker product structures, we apply the FEM Galerkin scheme to the equation (1.1) by means of the tensor-product piecewise linear finite elements

$$\{\psi_{\mathbf{i}}(x) := \psi_{i_1}(x_1) \cdots \psi_{i_d}(x_d)\}, \quad \mathbf{i} = (i_1, \dots, i_d), \quad i_{\ell} \in \mathcal{I}_{\ell} = \{1, \dots, n_{\ell}\},$$

$\ell = 1, \dots, d$ , where  $\psi_{i_{\ell}}(x_{\ell})$  are the univariate piecewise linear hat functions<sup>1</sup>. The unknown optimal design and control functions  $y$  and  $u$  in equation (1.1) are represented by  $y(x) = \sum_i y_i \psi_{\mathbf{i}}(x)$  and  $u(x) = \sum_i u_i \psi_{\mathbf{i}}(x)$ , with the coefficient vector  $\mathbf{y} = \{y_i\} \in \mathbb{R}^{N_d}$  and  $\mathbf{u} = \{u_i\} \in \mathbb{R}^{N_d}$ , respectively.

The  $N_d \times N_d$  stiffness matrix in the FEM Galerkin discretization of the elliptic operator (2.4) is constructed by the standard mapping of the multi-index  $\mathbf{i}$  into the long univariate index  $1 \leq i \leq N_d$  for the active degrees of freedom. For instance, we use the so-called big-endian convention for  $d = 3$  and  $d = 2$

$$\mathbf{i} \mapsto i := i_3 + (i_2 - 1)n_3 + (i_1 - 1)n_2n_3, \quad \mathbf{i} \mapsto i := i_2 + (i_1 - 1)n_2,$$

respectively. In what follows, we consider the case  $d = 3$  in more detail.

In our discretization scheme, we calculate the stiffness matrix by assembling the Kronecker product terms by using representation of the equation coefficient  $a(x)$  as an  $R$ -term sum of separable functions

$$a(x_1, x_2, x_3) = \sum_{k=1}^R a_k^{(1)}(x_1) a_k^{(2)}(x_2) a_k^{(3)}(x_3), \quad (2.5)$$

where the functions of univariate arguments,  $a_k^{(\ell)}(x_{\ell})$ , are supposed to be positive.

To that end, let us assume for the moment that the scalar diffusion coefficient  $a(x_1, x_2, x_3)$  can be represented in the separate form (rank-1 representation)

$$a(x_1, x_2, x_3) = a^{(1)}(x_1) a^{(2)}(x_2) a^{(3)}(x_3) > 0,$$

so that the target elliptic operator takes form

$$\mathcal{A} = - a_2(x_2) a_3(x_3) \frac{d}{dx_1} a_1(x_1) \frac{d}{dx_1} - a_1(x_1) a_3(x_3) \frac{d}{dx_2} a_2(x_2) \frac{d}{dx_2} - a_1(x_1) a_2(x_2) \frac{d}{dx_3} a_3(x_3) \frac{d}{dx_3}.$$

---

<sup>1</sup>Notice that the univariate grid size  $n_{\ell}$  designates the total problem size  $N_d = n_1 n_2 \cdots n_d$ .



diagonal matrix  $D_\ell = \text{diag}\{d_1, \dots, d_{n_\ell}\}$ ,  $\ell = 1, 2, 3$ , are defined as the row sum of the elements in the initial mass matrix  $S_\ell$ ,

$$d_i = s_{i,i-1} + s_{i,i} + s_{i,i+1}, \quad i = 1, \dots, n_\ell, \quad s_{1,0} = s_{n_\ell, n_\ell+1} = 0.$$

Then the corresponding stiffness matrix takes the form of Kronecker rank-3 representation,

$$A = A_1 \otimes D_2 \otimes D_3 + D_1 \otimes A_2 \otimes D_3 + D_1 \otimes D_2 \otimes A_3,$$

where  $D_\ell$ ,  $\ell = 1, 2, 3$ , denotes the diagonal matrices defined above. In the case of rank- $R$  separable coefficients, the stiffness matrix obeys the form of Kronecker rank- $3R$  structure as following

$$A = \sum_{k=1}^R (A_{1,k} \otimes D_{2,k} \otimes D_{3,k} + D_{1,k} \otimes A_{2,k} \otimes D_{3,k} + D_{1,k} \otimes D_{2,k} \otimes A_{3,k}). \quad (2.7)$$

Now given the matrix  $A$ , in the case of space-fractional control, one might be interested in the fast rank-structured solution of an equation with a fractional elliptic operator of non-local type (arising in applications to optimal control problems)

$$(A^\alpha + A^{-\alpha})u = F, \quad \alpha \in (0, 1],$$

in the spirit of the recent papers [18, 29]. However, for the expected level of generality concerning the equation coefficients in (2.5), we are not able to diagonalize the matrix  $A$  in a separable tensor product eigen-basis of one-dimensional elliptic operators as it was described in [18, 29]. That is due to the fact that the diagonal matrices  $D_\ell$  do not commute any more with the univariate stiffness matrices  $A_\ell$ . On the other hand, the full-format representation of non-local operators  $A^{\pm\alpha}$  becomes non-tractable for 3D discretizations on fine enough grids. Due to these observations, in what follows, we consider the case  $\alpha = 1$ .

The general model with  $\alpha \in (0, 1]$ , i.e. for fractional control, can be treated by the tensor based methods where the discretization scheme can be based on the contour integral representation, see for example [14, 20, 22]. This topic will be considered elsewhere.

In order to present an efficient tensor-vector multiplication  $Ax$  where  $A$  is given in Kronecker rank- $3R$  structure presented in (2.7), let  $x \in \mathbb{R}^N$  be a vector given in low-rank format, i.e.

$$x \approx \sum_{j=1}^S x_1^{(j)} \otimes x_2^{(j)} \otimes x_3^{(j)},$$

with vectors  $x_\ell^{(j)} \in \mathbb{R}_\ell^{n_\ell}$  and  $S \ll \min(n_1, n_2, n_3)$ . Then, a tensor-vector product can be computed by

$$\begin{aligned} & Ax \\ & \approx \left( \sum_{k=1}^R (A_1^{(k)} \otimes M_2^{(k)} \otimes M_3^{(k)} + M_1^{(k)} \otimes A_2^{(k)} \otimes M_3^{(k)} + M_1^{(k)} \otimes M_2^{(k)} \otimes A_3^{(k)}) \right) \left( \sum_{j=1}^S u_1^{(j)} \otimes u_2^{(j)} \otimes u_3^{(j)} \right) \\ & = \sum_{k=1}^R \sum_{m=1}^S (A_1^{(k)} u_1^{(m)} \otimes M_2^{(k)} u_2^{(m)} \otimes M_3^{(k)} u_3^{(m)} + M_1^{(k)} u_1^{(m)} \otimes A_2^{(k)} u_2^{(m)} \otimes M_3^{(k)} u_3^{(m)} \\ & \quad + M_1^{(k)} u_1^{(m)} \otimes M_2^{(k)} u_2^{(m)} \otimes A_3^{(k)} u_3^{(m)}). \end{aligned} \quad (2.8)$$

Aforementioned product (2.8) can be calculated in factorized form in  $O(d^2 R S n^2)$  flops, where  $n = \max(n_1, n_2, n_3)$ .

## 2.3 Setting up the equation for control and analysis of the condition number

We describe necessary first order conditions by a modification of the constructions in [18]. In the following discussion, we use the notations  $A_{FE}$  and  $A_{FD}$  for the finite element and finite difference matrices, respectively, discretizing the elliptic operator  $\mathcal{A}$ . Here the finite element matrix  $A = A_{FE}$  is constructed as described in §2.2, while the finite difference matrix  $A_{FD}$  is obtained from the latter by rescaling, see (2.11).

We consider a version of the control problem (2.1) constrained by (2.2), discretized by a FE method on a uniform grid in each dimension as described above,

$$\min_{\mathbf{y}, \mathbf{u}} = \frac{1}{2}(\mathbf{y} - \mathbf{y}_\Omega)^T M(\mathbf{y} - \mathbf{y}_\Omega) + \frac{\gamma}{2} \mathbf{u}^T M \mathbf{u} \quad (2.9)$$

$$\text{s. t. } A_{FE} \mathbf{y} = M \mathbf{u}, \quad (2.10)$$

where the coefficient vectors  $\mathbf{y}, \mathbf{y}_\Omega, \mathbf{u} \in \mathbb{R}^N$  denote the discretized state  $y$ , design  $y_\Omega$  and control  $u$ , respectively. The matrix  $M$  will be a mass matrix in the finite element case. To derive the FD scheme, we simplify the mass matrix to  $M = h^d I$  without loss of the asymptotic approximation rate. Then we arrive at the following scaling relation

$$A_{FD} = M^{-1} A_{FE} = h^{-d} A_{FE} \quad (2.11)$$

in the finite difference case. This translates the constraint equation (2.10) to the form  $A_{FD} \mathbf{y} = \mathbf{u}$ , while in the equation (2.9) the factor  $M$  can be skipped since the scaling by constant does not effect the minima of the functional.

Now setting up the Lagrangian function with the help of the discrete adjoint variable  $\mathbf{p}$ ,

$$L(\mathbf{y}, \mathbf{u}, \mathbf{p}) = \frac{1}{2}(\mathbf{y} - \mathbf{y}_\Omega)^T (\mathbf{y} - \mathbf{y}_\Omega) + \frac{\gamma}{2} \mathbf{u}^T \mathbf{u} + \mathbf{p}^T (A_{FD} \mathbf{y} - \mathbf{u}),$$

and differentiating it with respect to all three variables, we end up with the system of equations

$$\begin{bmatrix} E & O & A_{FD} \\ O & \gamma M & -E \\ A_{FD} & -E & O \end{bmatrix} \begin{pmatrix} \mathbf{y} \\ \mathbf{u} \\ \mathbf{p} \end{pmatrix} = \begin{pmatrix} \mathbf{y}_\Omega \\ \mathbf{0} \\ \mathbf{0} \end{pmatrix} \begin{matrix} \text{(I)} \\ \text{(II)} \\ \text{(III)} \end{matrix}.$$

This system contains the necessary first order optimality conditions for the minimizers solving the discretized optimal control problem (2.9), (2.10).

Then the state equation (III) can be solved for  $\mathbf{y}$ , yielding

$$\mathbf{y} = A_{FD}^{-1} \mathbf{u}. \quad (2.12)$$

Subsequently to solving (II) for  $\mathbf{p}$ , the adjoint equation (I) eventually provides an equation for the control  $\mathbf{u}$ , that is

$$(A_{FD}^{-1} + \gamma A_{FD}) \mathbf{u} = \mathbf{y}_\Omega. \quad (2.13)$$

The straightforward preconditioned iteration for solution of the initial equation for the control function,

$$(\gamma A + A^{-1}) u = F, \quad (2.14)$$

needs the calculation of the matrix times vector multiplication  $y_k = A^{-1} u_k$  for each current iterand  $u_k$ , which is equivalent to solving the linear system of equations  $A y_k = u_k$ . The latter equation can be solved by the PCG iteration with rank truncation at the optimal complexity scaling of the

order of  $O(n \log^q n)$ . However, the two-level embedded iteration might be too expensive in the case when the inner iteration requires a rather accurate solution.

To avoid the embedded iteration, we propose to solve the equivalent modified equation

$$(A^2 + I)u = AF. \quad (2.15)$$

In this case we only need the matrix vector multiplication with the squared matrix  $A^2$  and a spectrally equivalent preconditioner for  $A^2 + I$ . The latter is constructed by using a low Kronecker rank approximation of the inverse matrix  $(\Delta^2 + I)^{-1}$  by using the factorization in the 3D Fourier basis

$$(\Delta^2 + I)^{-1} = \mathcal{F}^*(A^2 + 1)^{-1}\mathcal{F},$$

which can be done by the similar techniques as in [18, 29]. From now on,  $\Delta$  denotes the discrete Laplacian on a tensor grid and  $A$  is the diagonal matrix of the corresponding eigenvalues.

Finally, for a spacing  $h \in (0, 1)$  we notice that the condition numbers of both matrices  $A + A^{-1}$  and  $A^2 + I$  are of the order of  $O(h^{-1})$  and  $O(h^{-2})$ , respectively, for the optimal scaling of the matrix  $A$ . In the following Lemma we consider two different scalings for the target matrix  $A$ .

**Lemma 2.1** (A) *Assume that  $\sigma(A) \in [h, 1/h]$ , then the condition number estimates hold*

$$\text{cond}(A + A^{-1}) = O(h^{-1}),$$

$$\text{cond}(A^2 + I) = O(h^{-2}).$$

(B) *Under the assumption  $\sigma(A) \in [1, 1/h^2]$  we obtain*

$$\text{cond}(A + A^{-1}) = O(h^{-2}),$$

$$\text{cond}(A^2 + I) = O(h^{-4}).$$

Proof. We consider the upper and lower bounds of the respective spectral functions

$$F_1(\lambda) = \lambda + \lambda^{-1} \quad \text{and} \quad F_2(\lambda) = \lambda^2 + 1, \quad \lambda \in \sigma(A).$$

For example, consider the function  $F_1(\lambda)$  in case (A). In this scenario it holds  $\min(F_1(\lambda)) = 2$ , while the maximal value,  $O(h^{-1})$ , is achieved on both endpoints of the spectrum  $\sigma(A)$ . Applying the similar arguments to other cases completes the proof. ■

In view of Lemma 2.1, a spectrally close preconditioner is mandatory for the efficient solution of both equations (2.14) and (2.15). In the following section, we construct and analyze the low  $K$ -rank spectrally close preconditioners for the system matrices  $A + A^{-1}$  and  $A^2 + I$ .

## 3 Preconditioning issues

### 3.1 Rank-structured spectrally close preconditioners: condition number estimates

We are interested in the construction of spectrally equivalent preconditioners for the matrices  $B = A + A^{-1}$  and  $S = A^2 + I$  in (2.14) and (2.15) in the form of low  $K$ -rank matrices. For both cases the resultant preconditioner is based on the simple spectrally close preconditioners constructed for the initial stiffness matrix  $A$ .

### 3.1.1 Preconditioning the stiffness matrix $A$

For the ease of presentation, first, we describe the construction of preconditioners for the two dimensional case, such that the target stiffness matrix is presented in the rank structured form

$$A = \sum_{k=1}^R (A_{1,k} \otimes D_{2,k} + D_{1,k} \otimes A_{2,k}), \quad (3.1)$$

where  $D_{\ell,k} = \text{diag}\{\mathbf{d}_{\ell,k}\} > 0$  are positive diagonal matrices and the tridiagonal matrices  $A_{\ell,k}$  are each spectrally equivalent to the 1D discrete Laplacian  $\Delta$  with equivalence constants  $a_{\ell,k}^{\pm} > 0$ ,  $\ell = 1, 2$ , that is it holds

$$a_{\ell,k}^- \Delta \leq A_{\ell,k} \leq a_{\ell,k}^+ \Delta, \quad \ell = 1, 2, \quad k = 1, \dots, R.$$

The constants  $a_{\ell,k}^{\pm} > 0$ ,  $\ell = 1, 2$ ,  $k = 1, \dots, R$  can be assumed to be a majorant and minorant to the respective coefficients  $a_{\ell}^k(x_{\ell})$ ,  $\ell = 1, 2$ ,  $k = 1, \dots, R$  as part of (2.4).

For preconditioning needs, we simplify the diagonal matrices by weighted identity matrices, where positive weights  $d_{\ell,k}^0$  are calculated as the average values of the corresponding diagonal vectors  $\mathbf{d}_{\ell,k} = \text{diag}\{D_{\ell,k}\} \in \mathbb{R}^n$ ,

$$d_{\ell,k}^0 = n^{-1} \langle \mathbf{d}_{\ell,k}, \mathbf{1} \rangle, \quad (3.2)$$

and introduce the constants

$$a_{\ell,k}^0 = \frac{1}{2} (a_{\ell,k}^+ + a_{\ell,k}^-) > 0, \quad k = 1, \dots, R.$$

Now agglomerating the anisotropy factors in both dimensions

$$a_{\ell}^0 = \sum_{k=1}^R a_{\ell,k}^0 \prod_{m=1; m \neq \ell}^d d_{m,k}^0, \quad \ell = 1, 2, \quad (3.3)$$

we construct the simple preconditioner  $B_1^{-1}$  with  $B_1 = A_1 + A_1^{-1}$  by using the anisotropic Laplacian

$$A_1 = a_1^0 \Delta_1 \otimes I_2 + a_2^0 I_1 \otimes \Delta_2, \quad (3.4)$$

where  $\Delta_1 = \Delta_2 = \Delta$ , so that the storage and matrix-vector multiplication with preconditioner  $B_1^{-1}$  can be implemented in  $O(n \log n)$  operations by low  $K$ -rank tensor decomposition of  $B_1^{-1}$  in the Fourier basis, see [29] for details. Likewise, the matrix  $A_1$  can be also used for the construction of preconditioners  $S_1^{-1}$  with  $S_1 = A_1^2 + I$  applied to the modified system matrix  $S$ .

The more advanced preconditioner  $B_2^{-1}$  with  $B_2 = A_2 + A_2^{-1}$ , as well as  $S_2^{-1} = (A_2^2 + I)^{-1}$ , based on the elliptic operator inverse with variable coefficients, see [29], are both constructed by using the matrix

$$A_2 = A_1^0 \otimes I_2 + I_1 \otimes A_2^0, \quad (3.5)$$

where

$$A_1^0 = \sum_{k=1}^R d_{2,k}^0 A_{1,k}, \quad A_2^0 = \sum_{k=1}^R d_{1,k}^0 A_{2,k}.$$

The matrix in (3.5) can be applied to enhance the convergence of PCG iteration in the situation with highly variable coefficients. In this case, following [29], we represent the low  $K$ -rank tensor decomposition of  $B_2^{-1}$  by using the factorization of  $B_2$  in the eigenbasis of the one-dimensional elliptic operators  $A_1^0$  and  $A_2^0$ . The asymptotic complexity estimate of the preconditioner includes

the term of the order of  $C_0 n^2$  with a small constant  $C_0$  in front of, which, does not fit (formally) the concept of  $O(n \log n)$ -complexity tensor based solver. However, in numerical tests we observe that the expense of matrix-vector multiplication operation of the complexity  $n^2$  remains negligible for moderate grid-size  $n$  and becomes noticeable only for the very large  $n$ .

The 3D analogies of both preconditioners  $B_1 = A_1 + A_1^{-1}$  and  $B_2 = A_2 + A_2^{-1}$  as well as  $S_1 = A_1^2 + I$  and  $S_2 = A_2^2 + I$  are based on the following constructions of matrices  $A_1$  and  $A_2$ . Given the stiffness matrix  $A$  in (2.7), the representations for both  $B_1$  and  $B_2$ , as well as for  $S_1$  and  $S_2$ , follow from the explicit expansions for the spectrally close to  $A$  matrices  $A_1$ , and  $A_2$ , defined by

$$A_1 = a_1^0 \Delta_1 \otimes I_2 \otimes I_3 + a_2^0 I_1 \otimes \Delta_2 \otimes I_3 + a_3^0 I_1 \otimes I_2 \otimes \Delta_3, \quad (3.6)$$

with the scaling constants,  $a_\ell^0 = \sum_{k=1}^R a_{\ell,k}^0 \prod_{m=1; m \neq \ell}^d d_{m,k}^0$ ,  $\ell = 1, 2, 3$ , and

$$A_2 = A_1^0 \otimes I_2 \otimes I_3 + I_1 \otimes A_2^0 \otimes I_3 + I_1 \otimes I_2 \otimes A_3^0, \quad (3.7)$$

where the matrices  $A_\ell^0 \in \mathbb{R}^{n \times n}$  are defined by

$$A_1^0 = \sum_{k=1}^R d_{2,k}^0 d_{3,k}^0 A_{1,k}, \quad A_2^0 = \sum_{k=1}^R d_{1,k}^0 d_{3,k}^0 A_{2,k}, \quad A_3^0 = \sum_{k=1}^R d_{1,k}^0 d_{2,k}^0 A_{3,k},$$

respectively. In 3D case the asymptotic complexity of preconditioner  $B_2$  is close to  $O(dn \log n)$  since the ‘‘complexity term’’  $C_1 n^2$  appears with a small constant and remains negligible in the practically interesting range of the univariate grid-size parameter  $n$ .

**Lemma 3.1** *Let the matrices  $A_1$  and  $A_2$  be given by (3.6) and (3.7), respectively, and the diagonal elements in (3.2) satisfy*

$$0 < d_{\ell,k}^- \leq \mathbf{d}_{\ell,k}[i] \leq d_{\ell,k}^+, \quad i = 1, \dots, n.$$

*Then the following spectral equivalence estimates hold*

$$(1 - q_A)(1 - q_D)^{d-1} A_1 \leq A \leq (1 + q_A)(1 + q_D)^{d-1} A_1, \quad (3.8)$$

where

$$q_A = \max_{\ell,k} \frac{a_{\ell,k}^+ - a_{\ell,k}^-}{a_{\ell,k}^+ + a_{\ell,k}^-} < 1,$$

does not depend on  $n$ . Furthermore, we have

$$(1 - q_D)^{d-1} A_2 \leq A \leq (1 + q_D)^{d-1} A_2, \quad (3.9)$$

where

$$q_D = \max_{\ell,k} \frac{d_{\ell,k}^+ - d_{\ell,k}^-}{d_{\ell,k}^+ + d_{\ell,k}^-} < 1$$

does not depend on  $n$ .

**Proof.** We split our proof into two arguments. To that end, we represent the averaged matrix  $A_2$  in the equivalent form

$$A_2 = \sum_{k=1}^R (A_{1,k} \otimes d_{2,k}^0 I_2 \otimes d_{3,k}^0 I_3 + d_{1,k}^0 I_1 \otimes A_{2,k} \otimes d_{3,k}^0 I_3 + d_{1,k}^0 I_1 \otimes d_{2,k}^0 I_2 \otimes A_{3,k}), \quad (3.10)$$

where the constants  $d_{\ell,k}^0$  denote the mean-value of the corresponding diagonals  $D_{\ell,k}$ , see (3.2). Now we apply the simple spectral bounds

$$(1 - q_D)d_{\ell,k}^0 I_\ell \leq D_{\ell,k} \leq (1 + q_D)d_{\ell,k}^0 I_\ell, \quad \ell = 1, 2, 3, \quad k = 1, \dots, R,$$

to obtain (for  $\ell = 1$ )

$$(1 - q_D)^{d-1} A_{1,k} \otimes d_{2,k} I_2 \otimes d_{3,k} I_3 \leq A_{1,k} \otimes D_{2,k} \otimes D_{3,k} \leq (1 + q_D)^{d-1} A_{1,k} \otimes d_{2,k} I_2 \otimes d_{3,k} I_3,$$

and similar for  $\ell = 2, 3$ . Summing up the above bounds over  $\ell = 1, 2, 3$  and  $k = 1, \dots, R$ , we arrive at the claim (3.9) for  $A_2$ .

To justify the estimate (3.8) we combine the previous argument with the corresponding spectral bounds for the tridiagonal matrices  $A_{\ell,k}$  in terms of the constant  $q_A$ ,

$$(1 - q_A)\Delta \leq A_{\ell,k} \leq (1 + q_A)\Delta, \quad \ell = 1, 2, 3; \quad k = 1, \dots, R,$$

which completes the proof.  $\blacksquare$

Following the arguments similar to those in [29], the condition number for both preconditioners  $B_1^{-1}$  and  $B_2^{-1}$ , as well as for  $S_1^{-1}$  and  $S_2^{-1}$ , applied to the system matrix  $B$  and  $S$ , respectively, can be estimated in terms of given quantities  $d_{\ell,k}^0$  and  $a_{\ell,k}^0$  and the corresponding equivalence constants for each of  $R$ -terms in (2.7). This issue is considered in the following sections.

### 3.1.2 Analysis of preconditioners for the system matrix $\mathbf{B} = \mathbf{A} + \mathbf{A}^{-1}$

Taking into account Lemma 3.1 the condition number for the preconditioned matrix  $B = A + A^{-1}$  can be estimated as follows

**Theorem 3.2** *Let the preconditioners be given by*

$$B_1 = A_1 + A_1^{-1} \quad \text{and} \quad B_2 = A_2 + A_2^{-1},$$

where the generating matrices  $A_1$  and  $A_2$  are defined by (3.6) and (3.7), respectively. Then under the above assumptions on the equation coefficients the following spectral bounds hold

$$\text{cond}(B_2^{-1}B) \leq \frac{\max\{(1 + q_D)^{d-1}, (1 - q_D)^{1-d}\}}{\min\{(1 + q_D)^{1-d}, (1 - q_D)^{d-1}\}} \equiv Q^{d-1}, \quad (3.11)$$

and

$$\text{cond}(B_1^{-1}B) \leq \frac{\max\{(1 + q_A)(1 + q_D)^{d-1}, (1 - q_A)^{-1}(1 - q_D)^{1-d}\}}{\min\{(1 + q_A)^{-1}(1 + q_D)^{1-d}, (1 - q_A)(1 - q_D)^{d-1}\}}, \quad (3.12)$$

for  $d = 2, 3$ , uniformly in  $n$ .

Proof. Based on Lemma 3.1 we derive the spectral bounds

$$(1 + q_D)^{1-d} A_2 \leq A^{-1} \leq (1 - q_D)^{1-d} A_2,$$

and

$$(1 + q_A)^{-1}(1 + q_D)^{1-d} A_1 \leq A^{-1} \leq (1 - q_A)^{-1}(1 - q_D)^{1-d} A_1,$$

then the results follow by combining the above estimates with (3.9) and (3.8), respectively.  $\blacksquare$

### 3.1.3 Analysis of preconditioners for the system matrix $S = A^2 + I$

In view of Lemma 3.1 the analysis of preconditioner for the modified matrix  $S = A^2 + I$  can be done along the same line. To that end, we use the preconditioners  $S_1 = A_1^2 + I$  and  $S_2 = A_2^2 + I$ , where the generating matrices  $A_1$  and  $A_2$  are defined as above. The following theorem holds.

**Theorem 3.3** *Let the preconditioners be given by*

$$S_1 = A_1^2 + I \quad \text{and} \quad S_2 = A_2^2 + I,$$

where the generating matrices  $A_1$  and  $A_2$  are defined by (3.6) and (3.7), respectively. Then under the above assumptions on the equation coefficients the following condition number bounds hold

$$\text{cond}(S_2^{-1}S) \leq \frac{(1 + q_D)^{2(d-1)}}{(1 - q_D)^{2(d-1)}}, \quad (3.13)$$

and

$$\text{cond}(S_1^{-1}S) \leq \frac{(1 + q_A)^2(1 + q_D)^{2(d-1)}}{(1 - q_A)^2(1 - q_D)^{2(d-1)}}, \quad (3.14)$$

for  $d = 2, 3$ , uniformly in  $n$ .

Proof. Lemma 3.1 ensures the following spectral bounds

$$(1 - q_A)^2(1 - q_D)^{2(d-1)}(A_1^2 + I) \leq A^2 + I \leq (1 + q_A)^2(1 + q_D)^{2(d-1)}(A_1^2 + I),$$

and

$$(1 - q_D)^{2(d-1)}(A_2^2 + I) \leq A^2 + I \leq (1 + q_D)^{2(d-1)}(A_2^2 + I),$$

then the result follows. ■

Theorem 3.3 proves that the condition number estimate (3.13) for preconditioner  $S_2$  provides stronger bound than that in (3.14) for  $S_1$  in view of the estimate

$$\frac{(1 + q_A)^2}{(1 - q_A)^2} > 1.$$

### 3.1.4 Comparison of preconditioners for two alternative formulations

Now we are able to compare the condition numbers for the preconditioned equations (2.14) and (2.15). The analysis of the right-hand side in equation (3.11) (in the following denoted by  $Q^{d-1}$ ) for the preconditioner  $B_2$  leads to the following three cases depending on respective value of max and min in the numerator and denominator:

$$Q^{d-1} = (1 + q_D)^{2(d-1)}, \quad Q^{d-1} = \frac{(1 + q_D)^{d-1}}{(1 - q_D)^{d-1}}, \quad Q^{d-1} = \frac{1}{(1 - q_D)^{2(d-1)}}.$$

This shows that in all cases we may expect the relations

$$\text{cond}(B_2^{-1}B) < \text{cond}(S_2^{-1}S).$$

The similar calculations lead to the estimate

$$\text{cond}(B_1^{-1}B) < \text{cond}(S_1^{-1}S).$$

We conclude that in all cases the PCG iteration for solving the initial equation (2.14) is expected to converge faster than in the case of modified formulation (2.15). On the other hand, the rank truncated matrix-vector multiplication with the system matrix  $A^2 + I$  can be implemented much faster by using the simple Horner scheme for multiplication of matrix polynomial with a vector,

$$A^2u = A(Au),$$

than that in the case with the system matrix  $A + A^{-1}$ . Indeed, in the latter case one needs the embedded PCG iteration to solve the equation  $Ay = u$ , required to calculate the action  $A^{-1}u$  at each iteration step.

Hence the comparison of numerical complexity for two equivalent formulations (2.14) and (2.15) is not a straightforward task in general since the trade-off between the reduced number of global PCG iterations vs. the reduced cost of matrix-vector operations, (i.e. the cost of one PCG iteration) mainly depends on the particular problem setting.

## 3.2 Enhancing the PCG iteration

In this section, we emphasize several issues which can be employed to optimize the convergence of the PCG iteration and to reduce the numerical cost of the whole solution process.

- I. With regard to the control of the number of PCG iterations, the optimal balance between the rank-truncation error  $\varepsilon_{trunc}$  and stopping criteria  $\varepsilon_{PCG}$  in the PCG iteration is important. In our numerical tests we therefore use the relation  $\varepsilon_{trunc} \leq C_0\varepsilon_{PCG}$  with  $C_0 \in [0.1, 0.01]$ .
- II. Using the *cascading* multigrid [30, 6] may reduce the iteration number on fine grids. The benefits of this approach are the following:
  - (a) There is only low extra cost for realization of the multigrid scheme compared with the single-grid one;
  - (b) The interpolation operator from coarse to fine grids applies only to 1D data (vectors) since the multivariate functions (grid-based solutions) are represented in the rank-structured separable form;
  - (c) The number of PCG iterations on the finest grid can be substantially reduced thanks to the good initial guess interpolated from coarser grid  $\Omega_h$  to finer grid  $\Omega_{h/2}$ ,

$$u_h \mapsto u_{h/2}$$

by using linear or cubic splines.

- III. The practical control of the FEM/FDM approximation in the considered control problems is a nontrivial task. Estimating the convergence rate of the FEM/FDM discretization in terms of the mesh-size can be performed on a sequence of grids, thus evaluating the true scale for the stopping criteria (in order to avoid over-iteration). We assume that the FEM/FDM approximate solution on the grid  $\Omega_h$  can be represented for small enough mesh-size  $h$  in the form

$$u_h = \hat{u}_h^* + \hat{C}_1 h^\alpha + O(h^{\alpha+1}), \quad \alpha > 0, \quad (3.15)$$

where the discrete functions  $\hat{u}_h^*$  and  $\hat{C}_1$  are the traces on the grid  $\Omega_h$  of the exact solution  $u^*(x)$  and the continuous function  $C_1(x)$ , respectively. Here the function  $C_1(x)$  does not depend

on the mesh parameter  $h$ . Then we readily obtain the decomposition of the inter-grid error decay by restricting  $u_{h/2}$  onto the coarser grid  $\Omega_h$ ,

$$u_h - u_{h/2} = (1 - 2^{-\alpha})\hat{C}_1 h^\alpha + O(h^{\alpha+1}).$$

Now calculating the ratio on two pairs of refined grids leads to the estimate

$$\frac{\|u_{2h} - u_h\|_2}{\|u_h - u_{h/2}\|_2} \approx 2^\alpha,$$

which indicates the decay rate of interest,  $\alpha > 0$ , where the norm in the nominator is calculated for the traces on the coarsest grid  $\Omega_{2h}$ , while denominator is evaluated on  $\Omega_h$ . The estimated parameter  $\alpha$  can be used in the error representation (3.15). In our numerical tests we observe the range of exponential  $\alpha \in [3/2; 2]$ . In most cases we arrive at the value  $\alpha = 2$  indicating the approximation error of the order of  $O(h^2)$  for the constructed FDM discretization scheme.

## 4 Numerical Results

In this section, we present numerical results for given 2D data. We consider the target operator  $A$  to be in a (low-)rank structured form as in (3.1). First, we are going to solve the illustrative example equation

$$Au = F \tag{4.1}$$

with respect to  $u$  to show that our low-rank PCG solution scheme making use of the algorithm introduced in [18] and presented in the Appendix of this paper indeed serves as a proper solver. Subsequently, we aim at solving equation (2.14) in order to solve control problem (2.9). In order to avoid embedded iterations, we solve the reformulated version of (2.14), namely

$$(\gamma A^2 + I)u = AF \tag{4.2}$$

for the control  $u$ .

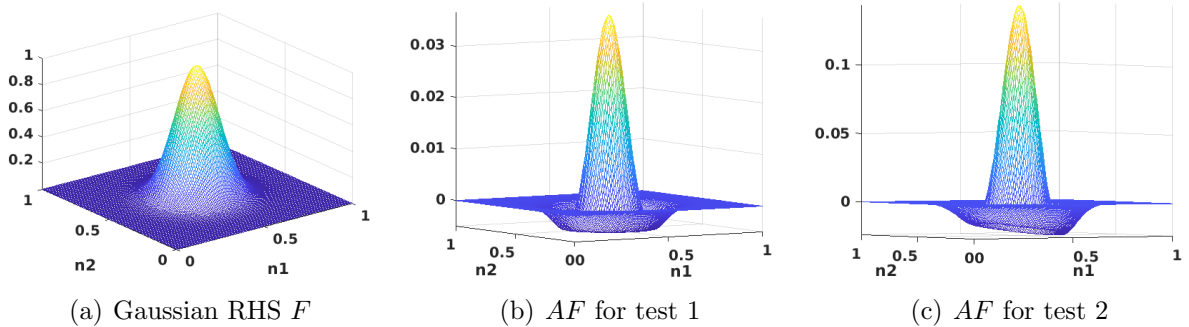


Figure 4.1: Gaussian-type right hand side (RHS)  $F$  and right hand side  $AF$  of equations (4.1) and (4.2), respectively.

For both equations, the optimal design  $F$  is given as the rank-1 representation of a Gaussian function, see figure 4.1. Ensuring low-rank representations of all involved operators throughout the solution scheme keeps the storage complexity comparatively low and enables us to solve equations

(4.1) and (4.2) on very fine grids, especially with regard to a possible application to 3D tensor data. This topic is discussed in more details at the end of this subsection. Within the PCG algorithm, we use a truncated SVD as rank truncation method and use  $\varepsilon_{trunc} = 10^{-8}$  as error threshold for truncation. We stop the algorithm whenever the relative residual is small enough, that is whenever  $\frac{\|Res\|}{\|F\|} = \varepsilon_{PCG} \leq 10^{-7}$  holds.

In the following, we present the results for two tests that differ in the rank-1 separable variable coefficients  $a(x_1, x_2) = \sum_{k=1}^R \prod_{m=1}^d a_m^k(x_m)$  that are part of the elliptic operator defined in (2.4). For the sake of clarity, we choose the coefficients to have rank  $R = 3$  throughout our tests, that is they are given by

$$a(x_1, x_2) = \sum_{k=1}^R a_1^k(x_1) a_2^k(x_2). \quad (4.3)$$

In *test 1*, we use the coefficients

$$a_1^k(x_1) = 1, \quad a_2^k(x_2) = 1, \quad k = 1, 2, 3, \quad (4.4)$$

resulting in the classic Laplace operator

$$\Delta = R(\Delta_1 \otimes I_2 + I_1 \otimes \Delta_2), \quad R = 3.$$

In *test 2*, we choose the coefficient functions to be given by

$$\begin{aligned} a_1^1(x_1) &= x_1 + 2, & a_2^1(x_2) &= 5x_2^2 + 2, \\ a_1^2(x_1) &= \sin(x_1) \cos(x_1) + 1, & a_2^2(x_2) &= 1, \\ a_1^3(x_1) &= 1, & a_2^3(x_2) &= \sin(4\pi x_2) + 2. \end{aligned} \quad (4.5)$$

Figure 4.2 provides a visualization for the total multi-dimensional diffusion coefficient (4.3) that is considered within the numerical examples for *test 2*. This total coefficient  $a(x_1, x_2)$  contains the one-dimensional rank-1 coefficients defined in (4.5).

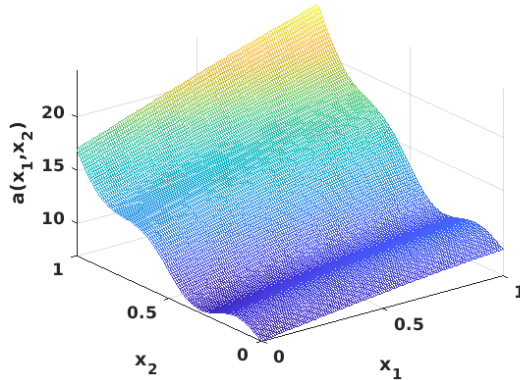


Figure 4.2: Total diffusion coefficient  $a(x_1, x_2)$  for *test 2* with single coefficients  $a_i^k(x_i)$ ,  $i = 1, 2$ ,  $k = 1, 2, 3$  defined in (4.5).

For both test settings and both equations (4.1) and (4.2), we present a numerical comparison of two different preconditioner approaches: When solving (4.1), we compare the respective inverse of  $A_1$  and  $A_2$ , that is we use  $\tilde{S}_1 = A_1^{-1}$  and  $\tilde{S}_2 = A_2^{-1}$  as preconditioners. For equation (4.2) we

compare the preconditioners  $S_1 = (A_1^2 + I)^{-1}$  and  $S_2 = (A_2^2 + I)^{-1}$ , that were introduced and discussed in section 3.1 and where  $A_1$  and  $A_2$  are respectively defined as in (3.4) and (3.5) via

$$A_1 = a_1^0 \Delta_1 \otimes I_2 + a_2^0 I_1 \otimes \Delta_2,$$

$$A_2 = A_1^0 \otimes I_2 + I_1 \otimes A_2^0,$$

where

$$A_1^0 = d_2^0 A_1, \quad A_2^0 = d_1^0 A_2,$$

anisotropy factors  $a_\ell^0$  given by (3.3) and weights  $d_\ell$  given by (3.2).

All preconditioning operators  $S_1$  and  $S_2$ ,  $\tilde{S}_1$ , and  $\tilde{S}_2$  are represented in low-rank structure where we choose the fixed rank parameter  $R_{precond} = 10$  throughout all tests.

## 4.1 Solving $Au = F$ and $(A^2 + I)u = AF$

In this section, we present the numerical results for the solution of equations (4.1) and (4.2) for an increasing number of grid points and the parameter  $\gamma = 1$ . The coarsest  $n \times n$  grid consists of  $n^2 = (2^5 - 1)^2 = 31^2 = 961$  grid points, whereas the finest grid consists of  $n^2 = (2^{12} - 1)^2 = 4095^2 = 16.769.025$  grid points.

First, we want to verify the usage of our low-rank pcg solver by comparing the time needed to solve equation (4.1),  $Au = F$ , by the low-rank pcg scheme to the time the direct backslash Matlab solver needs, that makes use of a Cholesky factorization. Test setting 1 is used, resulting in the classic Laplace operator. The Matlab solver is applied to the direct finite difference discretization of equation (4.1), that results in huge system matrices. It is worth to note that only by making use of sparse matrix structures it is possible to solve such huge systems up to a grid size of  $2047^2 = 4190209$  grid points with the direct Matlab solver. Table 4.1 shows the results of the comparison of the aforementioned solvers. It can be seen that for growing grid sizes, the rank-structured pcg solver clearly outperforms the direct Matlab solver with respect to time needed to solve (4.1). What is more, the low-rank pcg scheme ensures a consistent grid independent low rank of the solution operator. We therefore underline that ensuring low-rank structures of all involved operators within the pcg scheme makes a solution of (4.1) on very fine grids possible. It was not possible to solve the problem for grid sizes exceeding  $2047^2$  grid points with the direct Matlab solver on the above mentioned machine, while our low-rank pcg scheme could handle the respective large grid size of  $4095^2$  grid points. For more details on the required storage complexity that is linked to the solution rank, see the discussion at the end of this subsection.

In the following, we are going to analyze the performance of the low-rank pcg solution scheme for solving the problem-specific control equation (4.2), that is

$$(\gamma A^2 + I)u = AF.$$

Table 4.2 represents the results for solving equation (4.2) when using the coefficients defined for test 1, given by (4.4) and resulting in the operator  $A$  to be the classic Laplacian. Note that since all coefficients are chosen to be 1 in this case, both preconditioning approaches lead to the same preconditioning operator, that is  $S_1 = S_2$  since in this case it holds  $a_1^0 = a_1^0 = d_1^0 = d_2^0 = 1$ . Therefore, the results for both preconditioner styles are the same and there is no respective distinction in the table.

Table 4.3 represents the results for solving equation (4.2) using the coefficients defined for test 2, defined in (4.5). We show the differences in the results for different kinds of preconditioners  $S_1$  and  $S_2$  as described in the introductory part of this chapter. As theoretically shown in subsection

grid size	time pcg	sol. rank	time DM
$127^2$	0.0106	4	0,0375
$255^2$	0.0051	4	0,1271
$511^2$	0.0152	4	0,5363
$1023^2$	0.0250	4	2,0991
$2047^2$	0.0385	4	9,4740
$4095^2$	0.1069	4	–

Table 4.1: Total times in seconds needed by the rank-structured scheme and the direct Matlab (DM) solver to solve (4.1) with different numbers of grid points. The setting for test 1 and preconditioner  $\tilde{S}_1$  is used.

3.1, Theorem 3.3, we note that the numerical results confirm the superiority of a preconditioning operator in the style of  $A_2$  in contrast to using  $A_1$  since we notice a lower number of iterations needed to solve the problem, which is also associated to a faster convergence of the PCG algorithm.

Tables 4.2 and 4.3 both verify that the number of iterations needed by the pcg scheme to solve equation (4.2) does not (test 1) or only slightly (test 2) changes when a mesh refinement is done, implying that a successive performance of the low-rank pcg solver is ensured independently of the univariate grid size. Another important observation is that the rank of the solution matrix  $u$  does

grid size	# iter	time pcg (in sec.)	sol. rank
$31^2$	1	0.0037	4
$63^2$	1	0.0047	4
$127^2$	1	0.0092	4
$255^2$	1	0.0055	4
$511^2$	1	0.0113	4
$1023^2$	1	0.0309	4
$2047^2$	1	0.0792	4
$4095^2$	1	0.3479	4

Table 4.2: Results for solving equation (4.2) when using coefficients for test 1 and  $\gamma = 1$ . A cascadic mesh refinement is done.

not (test 1) or only observable slightly (test 2) change over different grid sizes, analogously to the case when solving test equation (4.1) (see table 4.1). That fact ensures that by using low-rank structures within the solution scheme, equations (4.1) and (4.2) can be solved for a huge number of grid points. Working with the full-format operator matrix  $A$  would require the storage of a  $n^2 \times n^2$  matrix, which is only tractable when exploiting sparse structures. As previously shown in table 4.1, this storage requirement cannot be handled by the used laptop (16GB RAM) when a grid size of  $2047^2$  grid points is exceeded. However, when using a low-rank decomposition of the respective operator, the storage can be reduced dramatically, resulting in a storage cost of the order  $O(dRn)$ , where in our tests  $d = 2$  and  $R$  denotes the rank of the solution  $u$  when solving (4.1) or (4.2). The aforementioned fact is the reason why it is important to ensure low-rank structures throughout the algorithm. The low-rank decomposition can be computed by using svd (in the 2D case) or the canonical tensor format (in the 3D case). For a more detailed discussion on this topic, also see

the recent paper of the authors [29]. Analyzing the time the pcg scheme needs in order to solve equation (4.2) for different univariate grid sizes  $n$ , we conclude that a nearly linear complexity scaling can be observed for both *test 1* and *test 2*. Figure 4.3 represents the control solution  $u$  of the problem-specific control equation (4.2) for two different test settings when using preconditioner style  $S_2$ , regularization parameter  $\gamma = 1$  and using a grid of size  $n_1 = n_2 = 255$  resulting in a total number of  $n^2 = 255^2$  grid points.

grid size	# iter		time pcg (in sec.)		time per iter		sol. rank	
	$S_1$	$S_2$	$S_1$	$S_2$	$S_1$	$S_2$	$S_1$	$S_2$
$31^2$	8	5	0.0328	0.0116	0.0041	0.0023	12	10
$63^2$	9	5	0.0581	0.0204	0.0065	0.0041	10	10
$127^2$	9	5	0.0854	0.0513	0.0095	0.0103	11	9
$255^2$	9	5	0.2150	0.0937	0.0239	0.0187	10	10
$511^2$	9	5	0.3159	0.1719	0.0351	0.0344	10	10
$1023^2$	9	5	0.5551	0.2763	0.0617	0.0553	11	10
$2047^2$	9	5	1.0924	0.7116	0.1214	0.1423	10	10
$4095^2$	9	5	2.7344	2.3951	0.3038	0.4790	10	10

Table 4.3: Results for solving equation (4.2) when using coefficients for test 2 and  $\gamma = 1$ . Two different preconditioner styles  $S_1$  and  $S_2$  are considered and a cascadic mesh refinement is done.

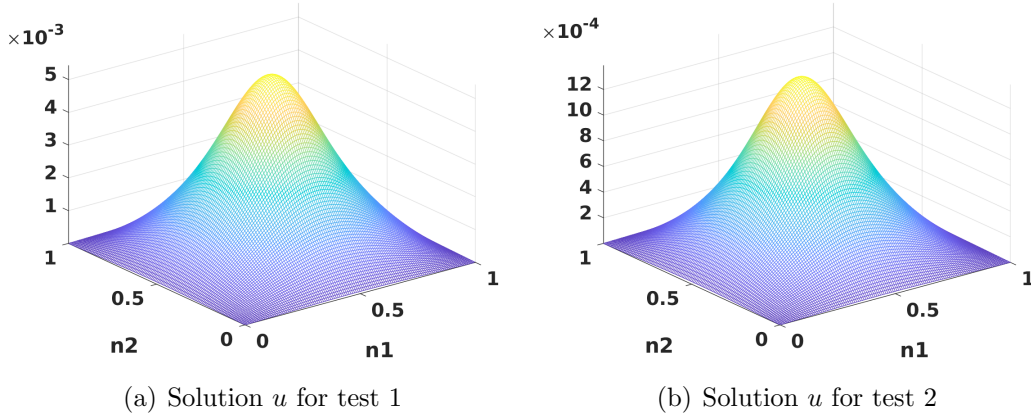


Figure 4.3: Solution  $u$  of problem-specific control equation (4.2) for different test settings 1 (left) and 2 (right), preconditioner  $S_2$ ,  $\gamma = 1$ , and  $n^2 = 255^2$  grid points.

**Remark 4.1** *In general, for the solution of optimal control problems of type (2.1), the regularization parameter  $\gamma$  is chosen to be very small,  $\gamma \ll 1$ , putting less weight on the regularization part of the objective function. However, our solution approach to the respective optimal control problem requires the solution of the control equation (4.2). For this equation, numerical tests indicate that the smaller parameter  $\gamma$  is chosen, the smaller the computational effort gets in order to solve equation (4.2). This is due to the fact that for  $\gamma \rightarrow 0$ , equation (4.2) approaches*

$$(N + I)u = F,$$

where  $N := \gamma A^2$  and  $N \xrightarrow{\gamma \rightarrow 0} 0$ .

## 4.2 Tests on the discretization convergence rate

In this subsection, we aim at identifying an explicit convergence rate for the FDM discretization scheme we use in our numerical test. As discussed in subsection 3.2, we want to estimate the rate in terms of the mesh-size, where accordingly to the statements in 3.2, we calculate the ratio on two pairs of solutions  $u$  on refined grids  $\Omega_{2h}$ ,  $\Omega_h$ , and  $\Omega_{h/2}$  as

$$c_h := \frac{\|u_{2h} - u_h\|_2}{\|u_h - u_{h/2}\|_2}, \quad (4.6)$$

where we expect  $c_h \approx 2^\alpha$ .

Note that  $u$  denotes the solution of equation (4.2) when  $\gamma = 1$ . For both *test 1* and *test 2*, we compute the ratio  $c_h$  numerically for grid sizes of size  $n^2 = (2^L - 1)^2$  for  $L = 6, \dots, 11$ , implying  $h = 1/n$  for  $\Omega = [0, 1]^2$ . For the sake of comparison, solutions  $u_{2h}$  and  $u_{h/2}$  are interpolated onto the grid specified by the discrete solution  $u_h$  when computing the ratio  $c_h$ . Table 4.4 displays the intergrid error ratio for the solutions  $u_{2h}, u_h, u_{h/2}$  on refined meshes.

The numerical results indicate a decay rate of  $\alpha = 2 > 0$ , leading to the estimate  $c_h \approx 2^2$ , which justifies the FDM approximation error of the order of  $O(h^2)$ .

grid size $n^2$	$63^2$	$127^2$	$255^2$	$511^2$	$1023^2$	$2047^2$
$c_h$ test 2 $S_2$	3,98	4,00	4,00	3,99	3,98	3,93
$c_h$ test 1	4,02	4,00	4,00	3,99	4,00	3,99

Table 4.4: Intergrid error ratio  $c_h$  for both *test 1* and *test 2*, where in *test 2* preconditioner style  $S_2$  is used.

## 4.3 Effects of a cascading multigrid approach

In this subsection, we want to investigate the impact of using a cascading multigrid scheme within our numerical pcg solution scheme. Therefore, we use the 1D solution data from grid  $\Omega_h$  in order to compute an initial guess for the refined grid  $\Omega_{h/2}$ , which is done by using a numerically cheap one-dimensional cubic spline prolongation operator

$$p : \mathbb{R}^{\Omega_h} \rightarrow \mathbb{R}^{\Omega_{h/2}}$$

that defines a polynomial of third degree.

Table 4.5 shows the impact of using the cascading multigrid approach when solving equation (4.2) within the setting of *test 2* when  $\gamma = 1$ . Analyzing the results and comparing them to the results presented in table 4.3, we notice that the number of needed iterations in order to solve equation (4.2) decreases for increasing grid sizes.

On the other hand, concerning the computational complexity, we note that for the finest grid consisting of  $4095^2$  grid points, the accumulated computational complexity for preconditioner  $S_2$  approximately matches, but for preconditioner  $S_1$  exceeds the time the algorithm needs to solve equation (4.2) without using a multigrid approach, see the respective *time pcg (in sec.)* in table 4.3. The accumulated complexity takes into account the time the algorithm needs in order to solve (4.2) on all previous grid sizes, leading to the initial guess that is subsequently used as initial guess

on the finest grid. The dates of table 4.5 also show that the time needed for a single iteration increases significantly for fine grids. This effect is discussed in details within the next section.

grid size	# iter		time pcg (in sec.)		time per iter		sol. rank	
	$S_1$	$S_2$	$S_1$	$S_2$	$S_1$	$S_2$	$S_1$	$S_2$
$31^2$	8	5	0.0842	0.0150	0.0404	0.0030	12	10
$63^2$	5	3	0.0518	0.0232	0.0104	0.0077	10	10
$127^2$	5	3	0.0810	0.0658	0.0162	0.0219	10	10
$255^2$	4	2	0.2010	0.0848	0.0503	0.0424	10	10
$511^2$	4	2	0.3667	0.1699	0.0917	0.0850	9	9
$1023^2$	4	2	0.7122	0.2902	0.1781	0.1451	9	9
$2047^2$	4	2	1.5562	0.6638	0.3890	0.3319	9	9
$4095^2$	3	1	2.0720	1.1479	0.6907	1.1479	9	9
<i>accumulated time</i>			5.3638	2.4606				

Table 4.5: Results for solving equation (4.2) when using coefficients for test 2, making use of a cascading multigrid scheme and choosing  $\gamma = 1$ . Two different preconditioner styles  $S_1$  and  $S_2$  are considered and a cascadic mesh refinement is done.

## 4.4 Rank propagation

In the preceding section, more precisely when analyzing table 4.5 and comparing it to the respective table 4.3 that represents the results when no multigrid approach is used, we notice a remarkable effect that arises when making use of a multigrid scheme in order to solve the problem-specific equation (4.2): While on the one hand, the number of iterations can be decreased to a minimum for fine grids, on the other hand, the time in seconds per iteration for finer grids when using a multigrid scheme increases and clearly exceeds the time per iteration when not using a multigrid scheme introduced in subsection 4.3 in order to solve (4.2). Therefore, we notice that the cumulative computational complexity of the multigrid scheme, obtained by summation the numerical costs over all grid levels, remains merely the same as for the unigrid solver applied on the finest grid.

This effect is due to the propagation of the rank of the initial guess operator (vector)  $\mathbf{X}^{(0)}$  used for the pcg scheme that is represented in the appendix. Please note that we refer to the number of columns of the respective operator by its *rank*. For every tensor-vector multiplication within the algorithm, the input tensor of K-rank  $R$  and vector of rank  $S$  multiply as defined in the multiplication scheme (2.8), resulting in rank  $RS$  for any tensor-vector product  $Ax$ . Furthermore, in our particular tests, we are interested in the solution of (4.2) that additionally requires the computation of a more advanced tensor-vector product  $(A^2 + I)u$ , that is computed by making use of the Horner scheme, implying a successive multiplication structure  $A(Au)$ . This method allows for a truncation-during-multiplication approach, where the rank  $RS$  originating from the first multiplication  $Au$  is immediately reduced to a rank  $r_\varepsilon \ll RS$  with respect to a truncation threshold  $\varepsilon_{trunc}$ . Hence, also taking into account special concatenation structures that are used for the numerical tests, the rank of the resulting complete tensor-vector product  $(A^2 + I)u$  can be estimated by  $(4Rr_\varepsilon + S)$ .

As already described in the introduction and the previous paragraph, we make use of a rank reduction procedure `trunc` that reduces the rank of the current operator to a given  $\varepsilon_{trunc}$ -threshold

within the multiplication scheme and after every step within Algorithm 1 in order to ensure trackability throughout the pcg scheme. In particular, in order to truncate the rank of the aforementioned product, we use a reduced SVD as truncation procedure `trunc` that due to considering a full matrix and an accuracy truncation threshold  $\varepsilon_{trunc}$  has a computational complexity of order  $O(\min(n^2(4Rr_\varepsilon + S), n(4Rr_\varepsilon + S)^2))$  strongly depending on the rank parameters  $R$  and  $S$  and therefore representing the most time-consuming part within the algorithm.

In order to understand the effect explained at the beginning of this subsection, we track the operator rank throughout the algorithm for test setting 2, preconditioner  $S_2$  and an example grid size of  $n^2 = 4095^2$  grid points when a multigrid scheme is used (MG) and when not (noMG). In the setting when no multigrid scheme is used, the nullvector  $\mathbf{X}_{noMG}^{(0)} \in \mathbb{R}^{n \times 1}$  serves as initial guess that implies rank  $S_{noMG}^{\mathbf{X}^{(0)}} = 1$ . When making use of a multigrid scheme, the pcg algorithm computes solutions to (4.2) starting on the coarsest grid of size  $n^2 = 31^2$  up to the finest grid of size  $n^2 = 4095^2$ , where the respective initial guess is computed as described in subsection 4.3, that is based on the solution of the respective previous grid. In our test, that leads to an initial guess  $\mathbf{X}_{MG}^{(0)} \in \mathbb{R}^{n \times 10}$  that implies rank  $S_{MG}^{\mathbf{X}^{(0)}} = 10$ . Note that in both settings, for the K-rank of the operator  $A$  it holds  $R_{MG} = R_{noMG} = 3$ .

Figure 4.4 represents the rank propagation throughout every step of the pcg scheme based on the respective initial guess rank  $S_{noMG}^{\mathbf{X}^{(0)}}$  and  $S_{MG}^{\mathbf{X}^{(0)}}$  for test 2, preconditioner  $S_2$  and grid size  $n^2 = 4095^2$ . Note that the multigrid scheme requires less iterations resulting in less single pcg steps. It is clearly observable that the rank spectrum when using a multigrid scheme significantly exceeds the rank spectrum when no multigrid scheme is used, which then also indicates a higher computational cost for the respective rank truncation operations by reduced SVD.

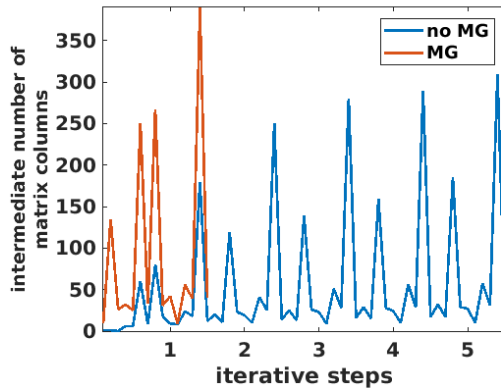


Figure 4.4: Rank propagation within the pcg scheme when using a multigrid scheme (red line) and when using no multigrid scheme (blue line) for test 2, preconditioner  $S_2$  and grid size  $n^2 = 4095^2$ .

Taking into account the results represented in tables 4.3, 4.5, and figure 4.4, we can summarize that ensuring low ranks throughout all steps of the algorithm, which in turn regulates the computational complexity of the truncated SVD, is the most important aspect in order to keep the total computational cost for solving equation (4.2) low. Furthermore, the characteristic of the multiplication scheme implies that low ranks are most likely to be kept low within the algorithm when the rank of the initial guess,  $S^{\mathbf{X}^{(0)}}$ , is low. A comparison of tables 4.3 and 4.5 indicates that the accumulated time for the multigrid iteration on finest grid is merely the same as the CPU time of the unigrid PCG iteration performed on the same grid though the MG algorithm converges in

only one iteration.

To conclude, we state that the advantages of ensuring a low rank of the initial guess  $\mathbf{X}^{(0)}$  and subsequently staying on a low rank manifold clearly outweigh the advantages of starting with a good initial guess within a multigrid scheme. It is worth to note that in our numerical tests, we also observed this effect when choosing smaller initial guess ranks  $1 < S_{MG} \ll 10$ .

## 5 Conclusion

In this paper, we introduce a tensor numerical method for the efficient solution of optimal control problems constrained by elliptic operators in  $\mathbb{R}^d$ ,  $d = 2, 3$ , with variable coefficients, which can be represented in the low rank separable form. The equation for the control function is discretized on large  $n^{\otimes d}$  grids and then solved by a PCG iteration with adaptive rank truncation. We construct and analyze the family of spectrally equivalent preconditioners by using tensor decomposition of matrix valued functions of the anisotropic Laplacian, which then are diagonalized in the Fourier basis.

Our numerical tests confirm that the discussed low rank PCG scheme serves as proper solver for the introduced problem class, as it outperforms considerably the direct Matlab solver especially on large grids. Furthermore, our numerical tests on the solution of the problem-specific control equation in 2D setting validate a nearly linear complexity scaling in the grid size  $n^2$ , where  $n \times n$  grids of size  $n^2 = 31^2$  up to  $n^2 = 4095$  are considered, while the number of iterations remains also stable throughout all grid sizes. A remarkable effect is that the  $K$ -rank  $R$  of the solution operator remains unaffected small throughout all grid sizes, ensuring a small storage complexity of order  $O(dRn)$  compared to the storage complexity that would be required in order to store the full solution operator of size  $n^2 \times n^2$ . Numerical investigations on the discretization convergence rate justify a FDM approximation error of order  $O(h^2)$  for our tests. What is more, all aforementioned results hold for both types of spectrally equivalent preconditioners that have been introduced in the course of the paper. However, the numerical tests validate the theoretical findings, stating that the initially defined operator-based preconditioner  $S_2$  outperforms the anisotropic Laplacian-type preconditioner  $S_1$ .

Last, we do an analysis on the integration of a cascadic multigrid method in our PCG scheme. The survey shows that integrating a multigrid scheme does not improve the computational complexity due to increasing ranks of the involved operators, however, the number of iterations can be efficiently decreased for increasing grid sizes. All in all, the results put stress on the importance of ensuring a low-rank structure of all involved quantities throughout the algorithm.

Finally, we notice that our approach can be generalized to the case of optimal control problems that contain fractional operators in constraints, however this problem class will be considered elsewhere.

## Appendix

We present the PCG iterative algorithm performed in a low-rank canonical format with the adaptive rank truncation for solving the linear system of equations for control function in  $\mathbb{R}^3$ , where the system matrix is given in low Kronecker rank format. As the rank truncation procedure, in our implementation we apply the reduced SVD algorithm since we work in a two-dimensional room. The algorithm has originally been introduced in [18].

---

**Algorithm 1** Preconditioned CG method in low-rank format

---

**Input:** Rank truncation procedure `trunc`, procedure `matvec` in the low  $K$ -rank format, preconditioner in low-rank format `precond`, right-hand side tensor  $\mathbf{B}$ , initial guess  $\mathbf{X}^{(0)}$ , rank tolerance parameter  $\varepsilon$ , maximal iteration number  $k_{\max}$

```
1:  $\mathbf{R}^{(0)} \leftarrow \mathbf{B} - \text{matvec}(\mathbf{X}^{(0)})$ 
2:  $\mathbf{Z}^{(0)} \leftarrow \text{precond}(\mathbf{R}^{(0)})$ 
3:  $\mathbf{Z}^{(0)} \leftarrow \text{trunc}(\mathbf{Z}^{(0)}, \varepsilon)$ 
4:  $\mathbf{P}^{(0)} \leftarrow (\mathbf{Z}^{(0)})$ 
5:  $k \leftarrow 0$ 
6: repeat
7:    $\mathbf{S}^{(k)} \leftarrow \text{matvec}(\mathbf{P}^{(k)})$ 
8:    $\mathbf{S}^{(k)} \leftarrow \text{trunc}(\mathbf{S}^{(k)}, \varepsilon)$ 
9:    $\alpha_k \leftarrow \frac{\langle \mathbf{R}^{(k)}, \mathbf{Z}^{(k)} \rangle}{\langle \mathbf{P}^{(k)}, \mathbf{S}^{(k)} \rangle}$ 
10:   $\mathbf{X}^{(k+1)} \leftarrow \mathbf{X}^{(k)} + \alpha_k \mathbf{P}^{(k)}$ 
11:   $\mathbf{X}^{(k+1)} \leftarrow \text{trunc}(\mathbf{X}^{(k+1)}, \varepsilon)$ 
12:   $\mathbf{R}^{(k+1)} \leftarrow \mathbf{R}^{(k)} - \alpha_k \mathbf{S}^{(k)}$ 
13:   $\mathbf{R}^{(k+1)} \leftarrow \text{trunc}(\mathbf{R}^{(k+1)}, \varepsilon)$ 
14:  if  $\mathbf{R}^{(k+1)}$  is sufficiently small then
15:    return  $\mathbf{X}^{(k+1)}$ 
16:    break
17:  end if
18:   $\mathbf{Z}^{(k+1)} \leftarrow \text{precond}(\mathbf{R}^{(k+1)})$ 
19:   $\mathbf{Z}^{(k+1)} \leftarrow \text{trunc}(\mathbf{Z}^{(k+1)}, \varepsilon)$ 
20:   $\beta_k \leftarrow \frac{\langle \mathbf{R}^{(k+1)}, \mathbf{Z}^{(k+1)} \rangle}{\langle \mathbf{Z}^{(k)}, \mathbf{R}^{(k)} \rangle}$ 
21:   $\mathbf{P}^{(k+1)} \leftarrow \mathbf{Z}^{(k+1)} + \beta_k \mathbf{P}^{(k)}$ 
22:   $\mathbf{P}^{(k+1)} \leftarrow \text{trunc}(\mathbf{P}^{(k+1)}, \varepsilon)$ 
23:   $k \leftarrow k + 1$ 
24: until  $k = k_{\max}$ 
```

**Output:** Solution  $\mathbf{X}$  of  $\text{matvec}(\mathbf{X}) = \mathbf{B}$

---

## Acknowledgment

This research has been supported by the German Research Foundation (DFG) within the *Research Training Group 2126: Algorithmic Optimization*, Department of Mathematics, Trier University, Germany.

## References

- [1] G. Allaire. *Numerical analysis and optimization: an introduction to mathematical modeling and numerical simulation*. Oxford University Press, 2007.
- [2] H. Antil and E. Otárola. *A FEM for an Optimal Control Problem of Fractional Powers of Elliptic Operators*. SIAM J. Control Optim., 53(6), pp.343-3456, 2015.
- [3] Harbir Antil, Andrei Drăgănescu, and Kiefer Green. *A note on multigrid preconditioning for fractional PDE-constrained optimization problems*. arXiv:2010.14600v1, 2016.

- [4] L. Banjai, J. M. Melenk, R. H. Nochetto, E. Otárola, A. J. Salgado and Ch. Schwab. *Tensor FEM for Spectral Fractional Diffusion*. Found. Comput. Math., (2018). <https://doi.org/10.1007/s10208-018-9402-3>.
- [5] A. Bonito, J. P. Borthagaray, R. H. Nochetto, E. Otarola, A. J. Salgado. *Numerical methods for fractional diffusion*. Computing and Visualization in Science (2018) 1-28.
- [6] F.A. Bornemann and P. Deuffhard. *The cascadic multigrid method for elliptic problems*. Numer. Math., 75:135-152, 1996.
- [7] A. Borzi and V. Schulz. *Multigrid methods for PDE optimization*. SIAM Review 51(2), 2009, 361-395.
- [8] A. Borzi and V. Schulz. *Computational optimization of systems governed by partial differential equations*. Soc. for Ind. and Appl. Math., Philadelphia, 2012.
- [9] L. De Lathauwer, B. De Moor, J. Vandewalle. *A multilinear singular value decomposition*. SIAM J. Matrix Anal. Appl., 21 (2000) 1253-1278.
- [10] J. C. De Los Reyes. *Numerical PDE-Constrained Optimization*. SpringerBriefs in Optimization, Springer, Berlin, 2015
- [11] S. Dolgov and I. V. Oseledets. *Solution of linear systems and matrix inversion in the TT-format*. SIAM J. Sci. Comput. 34 (5), 2011, pp. A2718-A2739.
- [12] S. Dolgov, J. Pearson, D. Savostyanov and M. Stoll. *Fast tensor product solvers for optimization problems with fractional differential equations as constraints*. Appl. Math. Comp., 273, 2016, 604-623.
- [13] B. Duan, R. Lazarov and J. Pasciak. *Numerical approximation of fractional powers of elliptic operators*. arXiv:1803.10055v1, 2018.
- [14] I. P. Gavrilyuk, W. Hackbusch and B. N. Khoromskij. *Data-Sparse Approximation to Operator-Valued Functions of Elliptic Operator*. Math. Comp. 73, (2003), 1297-1324.
- [15] W. Hackbusch. *Tensor spaces and numerical tensor calculus*. Springer, Berlin, 2012.
- [16] W. Hackbusch and B. N. Khoromskij. *Low-rank Kronecker product approximation to multi-dimensional nonlocal operators. Part I. Separable approximation of multi-variate functions*. Computing **76** (2006), 177-202.
- [17] S. Harizanov, R. Lazarov, and S. Margenov. *A survey on numerical methods for spectral space-fractional diffusion problems*. arXiv:2010.02717v1, 2020.
- [18] G. Heidel, V. Khoromskaia, B. N. Khoromskij and V. Schulz. *Tensor product method for fast solution of optimal control problems with fractional multidimensional Laplacian in constraints*. J Comput. Physics, 424, 109865, 2021.
- [19] R. Herzog and K. Kunisch. *Algorithms for PDE constrained optimization*. GAMM, 33 (2010), 163-176.
- [20] N. Hale, N. J. Higham, and L. N. Trefethen. *Computing  $A^\alpha$ ,  $\log(A)$ , and related matrix functions by contour integrals*. SIAM J. on Numerical Analysis, 46 (2), 2008, 2505-2523.
- [21] S. Harizanov, R. Lazarov, P. Marinov, S. Margenov and Ya. Vutov. *Optimal solvers for linear systems with fractional powers of sparse spd matrices*. Preprint arXiv:1612.04846v3, 2018.
- [22] N. J. Higham. *Functions of Matrices*. SIAM, Philadelphia, 2008.
- [23] V. Khoromskaia and B. N. Khoromskij. *Tensor Numerical Methods in Quantum Chemistry*. Research monograph, De Gruyter Verlag, Berlin, 2018.
- [24] B. N. Khoromskij. *Tensor Numerical Methods in Scientific Computing*. Research monograph, De Gruyter Verlag, Berlin, 2018.
- [25] B. N. Khoromskij and V. Khoromskaia. *Multigrid Tensor Approximation of Function Related Arrays*. SIAM J. Sci. Comp., 31(4), 3002-3026 (2009).

- [26] D. Kressner and C Tobler. *Krylov subspace methods for linear systems with tensor product structure*. SIAM J Matr. Anal. Appl., 31 (4), pp. 1688-1714.
- [27] M. Kwaśnicki. *Ten equivalent definitions of the fractional Laplace operator*. Functional Calculus and Applied Analysis, 20(1):7-51, 2017.
- [28] A. Lischke, G. Pang, M. Gulian, F. Song, Ch. Glusa, X. Zheng, Z. Mao, W. Cei, M. M. Meerschaert, M. Ainsworth, G. E. Karniadakis. *What is the fractional Laplacian?* arXiv:1801.09767v1, 2018.
- [29] B. Schmitt, B. Khoromskij, V. Khoromskaia, and V. Schulz. *Tensor Method for Optimal Control Problems Constrained by Fractional 3D Elliptic Operator with Variable Coefficients*. E-preprint, arXiv:2006.09314, 2020.
- [30] V.V. Shaidurov. *The multigrid methods for finite elements*. Kluwer Academic Publisher, Dordrecht, 1995.
- [31] F. Tröltzsch. *Optimal control of partial differential equations: theory, methods and applications*. AMS, Providence, Rhode Island, 2010.